Journal of applied physics, 104(4), 044904.
DOI: 10.1063/1.2970160

Modelling Shock Waves in Orthotropic Elastic Materials

Rade Vignjevic, James C. Campbell, Neil K. Bourne, Nenad Djordjevic
Crashworthiness, Impact and Structures Mechanics (CISM) Group,
School of Engineering, Cranfield University, Cranfield, Bedford MK43 0AL, UK
v.rade@cranfield.ac.uk

Abstract

A constitutive relationship for modeling of shock wave propagation in orthotropic materials is proposed for nonlinear explicit transient large deformation computer codes (hydrocodes). A procedure for separation of material volumetric compression (compressibility effects equation of state -EOS) from deviatoric strain effects is formulated which allows for the consistent calculation of stresses in the elastic regime as well as in the presence of shockwaves. According to this procedure the pressure is defined as the state of stress that results in only volumetric deformation, and consequently is a diagonal second order tensor.

As reported by Anderson[1] the shock response of an orthotropic material can not be accurately predicted using the conventional decomposition of the stress tensor into isotropic and deviatoric parts. This paper presents two different stress decompositions based on the assumption that the stress tensor is split into two components; one component due to volumetric strain and the other due to deviatoric strain. Both decompositions are rigorously derived. In order to test their ability to describe shock propagation in orthotropic materials, both algorithms were implemented in a hydrocode and their predictions compared with experimental plate impact data. The material considered was a carbon fibre reinforced epoxy material which was tested in both the through-thickness and longitudinal directions. The ψ decomposition showed good agreement with the physical behaviour of the considered material while the ζ decomposition significantly overestimated the longitudinal stresses.

1. Introduction

The use of composite materials in aerospace structures is on the increase. One of their main weaknesses is low impact resistance and significant reduction of compressive strength caused by impact related damage. To develop simulation tools capable of modelling high velocity impacts (characteristic loading rates between $1\times10^{3}s^{-1}$ and $1\times10^{8}s^{-1}$) on composites it is necessary to understand the formation and propagation of shock waves in composite materials. This problem is complicated by the complexity of the composite material structure and by the fact that mechanical properties of composite materials are dependent on loading rates and material orientation[2-4]. The consequence of this is that the shock wave velocity and state of stress behind the wave differ with material direction for identical impact cases.

Constitutive models developed for modelling of shock wave propagation in solids comprise two parts, an equation of state (EOS) which defines the response of the material to uniform compression (change of volume) and a deviatoric model which defines the response of the material to shear deformation (change of shape). The EOS controls the response of the material to shock loading. This separation of material response into volumetric and deviatoric strain components is well suited for isotropic materials, where the spherical part of the stress tensor $-P\delta_{ij}=C_{ijkl}\delta_{kl}\varepsilon_{pp}/3$, is a function only of the spherical part of the strain tensor. Furthermore, the principal axes of the stress and strain tensors are co-linear. In other words, components of stress and strain are proportional to each other and orthogonality between the volumetric and deviatoric components of strain is reflected in orthogonality

between the volumetric and deviatoric components of stress. It is simple to show that the definition of pressure as the average normal stress is the consequence of this orthogonality, i.e.

$$\begin{aligned} &\sigma_{ij} = -P\delta_{ij} + S_{ij} \\ &\sigma_{ij}\delta_{ij} = -P\delta_{kl}\delta_{kl} \\ &P = -\frac{\sigma_{ij}\delta_{ij}}{\delta_{kl}\delta_{kl}} \quad \rightarrow \quad P = -\sigma_{ii}/3 \\ &\delta_{ij}S_{ij} = 0 \end{aligned} \tag{1}$$

Using this definition of pressure Hooke's law for isotropic materials can be expressed as

$$\sigma_{ij} = \lambda\varepsilon_{kk}\delta_{ij} + 2\mu\varepsilon_{ij} = \left(\lambda + \frac{2}{3}\mu\right)\delta_{ij}\varepsilon_{kk} + 2\mu\varepsilon_{ij}^{d} = -P\delta_{ij} + S_{ij} \tag{2}$$

where S_{ij} and ε_{ij}^{d} are the deviatoric parts of the stress and strain tensor respectively and, λ and μ are Lame parameters.

The conventional decomposition, equation (2) does not hold for orthotropic materials as both the spherical and deviatoric parts of the stress tensor each induce volumetric and deviatoric strain. Using this standard decomposition to model shock propagation in orthotropic materials does not accurately predict the material behaviour. The method for improvement of the relation between EOS and the isotropic state of strain for orthotropic materials proposed by Anderson[1], who derived an expression for pressure as a function of the volumetric and deviatoric components of the strain tensor has been frequently used in hydrocodes.

This paper investigates two different stress decompositions for orthotropic materials applied to the modelling of the propagation of shock waves in composite materials. In deriving the decompositions, one constraint was that the proposed constitutive model would use existing types of shock equations of state and related material data derived from plate impact tests, e.g. [2-5]. The proposed procedure is developed for an incremental strain formulation within explicit time integration scheme. It is applicable to either finite difference or finite element semi-discretisation.

2. Constitutive stress - strain relationship for orthotropic materials

The relative simplicity in modelling the elastic behaviour in isotropic materials is a consequence of the fact that the material is fully characterized by two parameters. In the case of elastic orthotropic materials, nine parameters are required to define the stress strain relationship using either stiffness, equation (3), or compliance matrices - equation (4).

$$\sigma_{ij} = C_{ijkl}\varepsilon_{kl} \tag{3}$$

$$\varepsilon_{ij} = C_{ijkl}^{-1}\sigma_{kl} = B_{ijkl}\sigma_{kl} \tag{4}$$

Equations (3,4) can be rewritten using Voigt notation as $\sigma_p = C_{pq}\varepsilon_q$ and $\varepsilon_q = C_{pq}^{-1}\sigma_p = B_{qp}\sigma_p$ where $\varepsilon_q = (2-\delta_{kl})\varepsilon_{kl}$. The relationships between indices *p,q* and *i,j,k,l* are define by the following expressions $p = \delta_{ij}i + (1-\delta_{ij})(9-i-j)$, $q = \delta_{kl}k + (1-\delta_{kl})(9-k-l)$. The material stiffness tensor C_{ijkl} written in Voigt notation has the following form:

$$\begin{bmatrix} C_{1111} & C_{1122} & C_{1133} & 0 & 0 & 0 \\ C_{1122} & C_{2222} & C_{2233} & 0 & 0 & 0 \\ C_{1133} & C_{2233} & C_{3333} & 0 & 0 & 0 \\ 0 & 0 & 0 & C_{2323} & 0 & 0 \\ 0 & 0 & 0 & 0 & C_{1313} & 0 \\ 0 & 0 & 0 & 0 & 0 & C_{1212} \end{bmatrix} = \begin{bmatrix} C_{11} & C_{12} & C_{13} & 0 & 0 & 0 \\ C_{12} & C_{22} & C_{23} & 0 & 0 & 0 \\ C_{13} & C_{23} & C_{33} & 0 & 0 & 0 \\ 0 & 0 & 0 & C_{44} & 0 & 0 \\ 0 & 0 & 0 & 0 & C_{55} & 0 \\ 0 & 0 & 0 & 0 & 0 & C_{66} \end{bmatrix} =$$

$$\frac{1}{\Delta}\begin{bmatrix} \frac{1-\nu_{23}\nu_{32}}{E_2E_3} & \frac{\nu_{21}+\nu_{23}\nu_{31}}{E_2E_3} & \frac{\nu_{31}+\nu_{21}\nu_{32}}{E_2E_3} & 0 & 0 & 0 \\ \frac{\nu_{12}+\nu_{32}\nu_{13}}{E_1E_3} & \frac{1-\nu_{13}\nu_{31}}{E_1E_3} & \frac{\nu_{32}+\nu_{12}\nu_{31}}{E_1E_3} & 0 & 0 & 0 \\ \frac{\nu_{13}+\nu_{12}\nu_{23}}{E_1E_2} & \frac{\nu_{23}+\nu_{13}\nu_{21}}{E_1E_2} & \frac{1-\nu_{12}\nu_{21}}{E_1E_2} & 0 & 0 & 0 \\ 0 & 0 & 0 & G_{23}\Delta & 0 & 0 \\ 0 & 0 & 0 & 0 & G_{31}\Delta & 0 \\ 0 & 0 & 0 & 0 & 0 & G_{12}\Delta \end{bmatrix} \quad (5)$$

Where: $\Delta = \frac{1-\nu_{12}\nu_{21}-\nu_{23}\nu_{32}-\nu_{31}\nu_{13}-2\nu_{21}\nu_{32}\nu_{13}}{E_1E_2E_3}$

The material compliance tensor can be expressed in a similar form:

$$\begin{bmatrix} B_{1111} & B_{1122} & B_{1133} & 0 & 0 & 0 \\ B_{1122} & B_{2222} & B_{2233} & 0 & 0 & 0 \\ B_{1133} & B_{2233} & B_{3333} & 0 & 0 & 0 \\ 0 & 0 & 0 & B_{2323} & 0 & 0 \\ 0 & 0 & 0 & 0 & B_{1313} & 0 \\ 0 & 0 & 0 & 0 & 0 & B_{1212} \end{bmatrix} = \begin{bmatrix} B_{11} & B_{12} & B_{13} & 0 & 0 & 0 \\ B_{12} & B_{22} & B_{23} & 0 & 0 & 0 \\ B_{13} & B_{23} & B_{33} & 0 & 0 & 0 \\ 0 & 0 & 0 & B_{44} & 0 & 0 \\ 0 & 0 & 0 & 0 & B_{55} & 0 \\ 0 & 0 & 0 & 0 & 0 & B_{66} \end{bmatrix} =$$

$$= \begin{bmatrix} \frac{1}{E_1} & -\frac{\nu_{21}}{E_2} & -\frac{\nu_{31}}{E_3} & 0 & 0 & 0 \\ -\frac{\nu_{12}}{E_1} & \frac{1}{E_2} & -\frac{\nu_{32}}{E_3} & 0 & 0 & 0 \\ -\frac{\nu_{13}}{E_1} & -\frac{\nu_{23}}{E_2} & \frac{1}{E_3} & 0 & 0 & 0 \\ 0 & 0 & 0 & \frac{1}{G_{23}} & 0 & 0 \\ 0 & 0 & 0 & 0 & \frac{1}{G_{31}} & 0 \\ 0 & 0 & 0 & 0 & 0 & \frac{1}{G_{12}} \end{bmatrix} \quad (6)$$

where: E_i are Young's moduli, $G_{ij}, i \neq j$ are shear elastic moduli, ν_{ij} are Poisson ratios

3. Alternative decomposition of stress tensor for orthotropic materials

The issue of the stress decomposition was considered by Anderson[1] in relation to wave propagation in anisotropic materials. He demonstrates that for an anisotropic material pressure depends not only on volumetric strain but also on the deviatoric strain components, therefore the decomposition used for isotropic materials is not applicable.

$$
\begin{aligned}
P=&-\frac{1}{9\beta}\{E_1(1-\nu_{23}\nu_{32})+E_2(1-\nu_{13}\nu_{31})+E_3(1-\nu_{12}\nu_{21})+\\
&+2\left[E_1(\nu_{21}+\nu_{31}\nu_{23})+E_1(\nu_{31}+\nu_{21}\nu_{32})+E_2(\nu_{32}+\nu_{31}\nu_{12})\right]\}\varepsilon+\\
&+\frac{1}{3\beta}\{E_1(1-\nu_{23}\nu_{32})+E_1(\nu_{21}+\nu_{31}\nu_{23})+E_1(\nu_{31}+\nu_{21}\nu_{32})\}\varepsilon_{11}^d+\\
&+\frac{1}{3\beta}\{E_2(\nu_{21}+\nu_{31}\nu_{23})+E_2(1-\nu_{13}\nu_{31})+E_2(\nu_{32}+\nu_{12}\nu_{31})\}\varepsilon_{22}^d+\\
&+\frac{1}{3\beta}\{E_3(\nu_{31}+\nu_{21}\nu_{32})+E_3(\nu_{32}+\nu_{12}\nu_{31})+E_3(1-\nu_{12}\nu_{21})\}\varepsilon_{33}^d
\end{aligned}
\tag{7}
$$

where $\beta=1-\nu_{12}\nu_{21}-\nu_{13}\nu_{31}-\nu_{23}\nu_{32}-\nu_{12}\nu_{23}\nu_{31}-\nu_{13}\nu_{21}\nu_{32}$ and $\varepsilon=\varepsilon_{11}+\varepsilon_{22}+\varepsilon_{33}$.

This approach does not accurately predict levels of stress behind a shock wave when modelling orthotropic materials when a shock equation of state is used. An example of this can be seen in the results shown in section 5.

As already stated, in the case of isotropic materials isotropic states of strain induce isotropic states of stress (pressure) and they are directly related through bulk modulus. An equivalent relationship cannot be defined for orthotropic materials. If one maintains the assumption that pressure is the state of stress induced by volumetric strain (uniform compression or expansion) then a more general definition of pressure is required. This leads to a number of possible definitions of pressure as a vector in the principal stress space which, for orthotropic materials, does not coincide with the hydrostat. To explore this statement further one can consider the following two possibilities.

3.1 Decomposition 1 or ψ decomposition

Stress due to the isotropic component of strain (or isotropic strain pressure) is defined as

$$-\hat{P}\psi_{ij}=C_{ijkl}\delta_{kl}\varepsilon_{ss}/3=C_{ijkk}\varepsilon_v \tag{8}$$

Where: $\psi_{ij}=0 \quad \forall \quad i\neq j, \quad \psi_{ij}\neq 0 \quad \forall \quad i=j$, $\varepsilon_v=\varepsilon_{ss}/3$.

From equation (8) parameter $\hat{P}$ and tensor ψ_{ij} can be expressed as

$$-\hat{P}=\varepsilon_v\sqrt{\frac{1}{\psi_{st}\psi_{st}}C_{ijkk}C_{ijll}} \tag{9}$$

$$\psi_{ij}=-C_{ijkk}\varepsilon_v/\hat{P}=\frac{C_{ijkk}}{\sqrt{\frac{1}{\psi_{st}\psi_{st}}C_{prkk}C_{prll}}} \tag{10}$$

To uniquely define $\hat{P}$ and tensor ψ_{ij} it is necessary to define the double contraction $\psi_{st}\psi_{st}$. One possibility is to make the assumption that $\psi_{st}\psi_{st}=3$, the consequences of which are discussed below.

Note, that in following this assumption the tensor ψ_{ij} is fully defined by the material elastic stiffness properties.

Equations (8, 9 and 10) when written in Voigt notation become equations (11, 12 and 13) respectively:

$$\hat{P}\begin{Bmatrix}\psi_1\\ \psi_2\\ \psi_3\\ 0\\ 0\\ 0\end{Bmatrix} = -\begin{bmatrix} C_{11} & C_{12} & C_{13} & 0 & 0 & 0\\ C_{12} & C_{22} & C_{23} & 0 & 0 & 0\\ C_{13} & C_{23} & C_{33} & 0 & 0 & 0\\ 0 & 0 & 0 & C_{44} & 0 & 0\\ 0 & 0 & 0 & 0 & C_{55} & 0\\ 0 & 0 & 0 & 0 & 0 & C_{66}\end{bmatrix}\begin{Bmatrix}\varepsilon_v\\ \varepsilon_v\\ \varepsilon_v\\ 0\\ 0\\ 0\end{Bmatrix} \tag{11}$$

The scalar $\hat{P}$ which defines the magnitude of pressure is defined as

$$\hat{P} = -\sqrt{\frac{\left(C_{11}+C_{12}+C_{13}\right)^2+\left(C_{12}+C_{22}+C_{23}\right)^2+\left(C_{13}+C_{23}+C_{33}\right)^2}{3}}\varepsilon_v = -3K_\psi\varepsilon_v \tag{12}$$

Note that parameter K_ψ reduces to the conventional bulk modulus, i.e. $K_\psi = E/(3(1-2\nu))$ in the limit of material isotropy.

$$\psi_{(ii)} = \frac{C_{i1}+C_{i2}+C_{i3}}{\sqrt{\frac{\left(C_{11}+C_{12}+C_{13}\right)^2+\left(C_{12}+C_{22}+C_{23}\right)^2+\left(C_{13}+C_{23}+C_{33}\right)^2}{3}}} \tag{13}$$

In the above equation repeated indices in brackets indicate no summation. It is important to note that in the case of isotropic materials ψ_{ij} becomes δ_{ij} and the stress decomposition reduces to the conventional decomposition for isotropic materials. Tensor ψ_{ij} defines points in stress space which induce an isotropic strain state in the material.

An alternative definition of the tensor ψ_{ij} can be derived by using equation (8) to determine parameter $\hat{P}$ from the following relationship, $\det\left|-\hat{P}\psi_{ij}\right| = \det\left|C_{ijkk}\varepsilon_v\right|$. This approach has not been considered in this paper.

Using defined parameters, the decomposition of the stress tensor can be done as follows:

$$\sigma_{ij} = C_{ijkl}\delta_{kl}\varepsilon_{ss}/3 + C_{ijkl}\varepsilon_{kl}^d = -\hat{P}\psi_{ij} + \hat{S}_{ij} \tag{14}$$

It is important to notice that in this decomposition the part of the stress tensor $\hat{P}\psi_{ij}$ due to isotropic strain is not orthogonal to the part of the stress tensor $\hat{S}_{ij}$ due to deviatoric strain, i.e. $\hat{P}\psi_{ij}\hat{S}_{ij} \neq 0$. If the stress tensor is divided into two parts where $\tilde{P}\psi_{ij}\tilde{S}_{ij} = 0$ one can write:

$$\sigma_{ij} = -\hat{P}\psi_{ij} + \hat{S}_{ij} = -\tilde{P}\psi_{ij} + \tilde{S}_{ij} \tag{15}$$

To determine $\tilde{P}$ and $\tilde{S}_{ij}$ equation (15) should be multiplied by ψ_{ij}

$$\sigma_{ij}\psi_{ij} = -\hat{P}\psi_{ij}\psi_{ij} + \hat{S}_{ij}\psi_{ij} = -\tilde{P}\psi_{ij}\psi_{ij} + \tilde{S}_{ij}\psi_{ij} \tag{16}$$

Using the assumption that $\tilde{S}_{ij}\psi_{ij}=0$ equation (16) yields $\tilde{P}$ as:

$$\tilde{P}=\hat{P}-\frac{\hat{S}_{ij}\psi_{ij}}{\psi_{kl}\psi_{kl}}=\hat{P}-\hat{S}=-\frac{\sigma_{ij}\psi_{ij}}{3} \tag{17}$$

Substituting equation (17) into (15) yields the expression for the deviatoric part of the stress tensor:

$$\tilde{S}_{ij}=\hat{S}_{ij}-\frac{\hat{S}_{kl}\psi_{kl}}{\psi_{sr}\psi_{sr}}\psi_{ij}=\hat{S}_{ij}-\hat{S}\psi_{ij} \qquad \tilde{S}_{ij}=\sigma_{ij}-\frac{\sigma_{kl}\psi_{kl}}{\psi_{sr}\psi_{sr}}\psi_{ij}=\sigma_{ij}+\tilde{P}\psi_{ij} \tag{18}$$

Similarly, $\hat{S}$ can be obtained directly from the normality condition $\tilde{S}_{ij}\psi_{ij}=0$ as

$$\begin{aligned}&\hat{S}_{ij}=\hat{S}\psi_{ij}+\tilde{S}_{ij} \quad /\psi_{ij}\\ &\hat{S}_{ij}\psi_{ij}=\hat{S}\psi_{ij}\psi_{ij}\\ &\hat{S}=\frac{\hat{S}_{ij}\psi_{ij}}{\psi_{kl}\psi_{ikl}}=\frac{\hat{S}_{ij}\psi_{ij}}{3}\end{aligned} \tag{19}$$

The proposed division of the stress tensor derived above reduces to the conventional division given in equation (1) in the case of isotropic materials.

3.2 Decomposition 2 or ζ decomposition

Following a similar process one can define a second order tensor ζ_{ij}, which satisfies equation (20), orthogonal to the part of the stress tensor $\hat{S}_{ij}=C_{ijkl}\varepsilon^{d}_{kl}$ induced by the deviatoric strain tensor.

$$\hat{S}_{ij}\zeta_{ij}=0 \tag{20}$$

One way for calculation of ζ_{ij} is given below

$$\begin{aligned}&\hat{S}_{ij}\zeta_{ij}=C_{ijkl}\zeta_{ij}\varepsilon^{d}_{kl}=\delta_{kl}\varepsilon^{d}_{kl}=0 \quad\leftrightarrow\quad C_{ijkl}\zeta_{ij}=\delta_{kl}\\ &\zeta_{ij}=C^{-1}_{ijkl}\delta_{kl}=B_{ijkl}\delta_{kl}\end{aligned} \tag{21}$$

Where $\zeta_{ij}=0 \quad \forall \quad i\neq j, \quad \zeta_{ij}\neq 0 \quad \forall \quad i=j$ and $\zeta_{ij}\zeta_{ij}=3$. The tensor ζ_{ij} is fully defined with the material elastic compliance properties, i.e.

$$\zeta_{(ii)}=\frac{B_{i1}+B_{i2}+B_{i3}}{\sqrt{\frac{\left(B_{11}+B_{12}+B_{13}\right)^2+\left(B_{12}+B_{22}+B_{23}\right)^2+\left(B_{13}+B_{23}+B_{33}\right)^2}{3}}} \tag{22}$$

Repeated indices in brackets indicate no summation. It is important to note that in the case of isotropic materials ζ_{ij} becomes δ_{ij} and the stress decomposition reduces to the conventional decomposition for isotropic materials. Tensor ζ_{ij} is perpendicular to a plane in stress space on which all points induce deviatoric strain states in the material.

Tensor ζ_{ij} allows for a second type of stress tensor decomposition to be defined. In this decomposition isotropic strain induces pressure $\underset{\sim}{P}\zeta_{ij}$ and contributes to the deviatoric components of stress $\underset{\sim}{S}_{ij}$. Starting from the ψ decomposition and the definition of ζ_{ij} tensor one can write:

$$\sigma_{ij}=-\tilde{P}\psi_{ij}+\tilde{S}_{ij}=-\underset{\sim}{P}\zeta_{ij}+\underset{\sim}{S}_{ij} \tag{23}$$

Multiplying equation (23) by ζ_{ij} and substituting $\underset{\sim}{S}_{ij}\zeta_{ij}=0$ yields

$$\sigma_{ij}\zeta_{ij} = -\tilde{P}\psi_{ij}\zeta_{ij} + \tilde{S}_{ij}\zeta_{ij} = -\underset{\sim}{P}\zeta_{ij}\zeta_{ij} = -3\underset{\sim}{P}$$

$$\underset{\sim}{P} = -\frac{\sigma_{ij}\zeta_{ij}}{3} = \frac{\tilde{P}\psi_{ij}\zeta_{ij}}{3} - \frac{\tilde{S}_{ij}\zeta_{ij}}{3} \tag{24}$$

Substituting equation (24) into equation (23) yields the corresponding deviatoric part of the stress tensor

$$\underset{\sim}{S}_{ij} = \tilde{S}_{ij} - \tilde{P}\psi_{ij} + \left[\frac{\tilde{P}\psi_{kl}\zeta_{kl}}{3} - \frac{\tilde{S}_{kl}\zeta_{kl}}{3}\right]\zeta_{ij} \tag{25}$$

This completes the derivation of the second decomposition of the stress tensor for orthotropic materials. Graphical interpretation of two decompositions is given in Fig. 1.

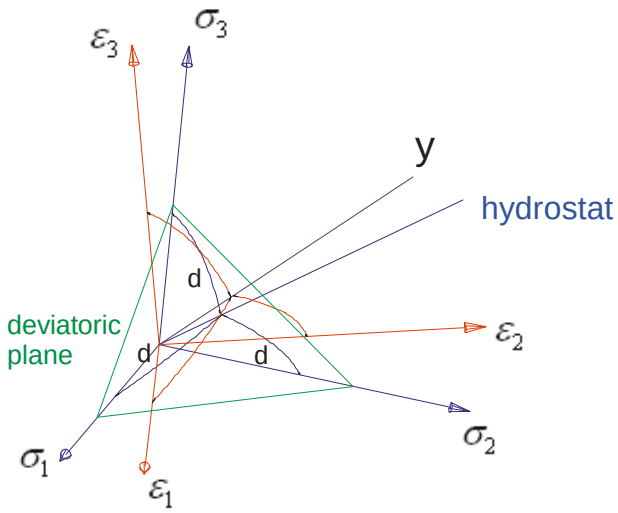

FIGURE 1. Schematic representation of the ψ vector in the principle stress and strain spaces

The two stress decompositions described above were incorporated into the Lawrence Livermore National Laboratory (LLNL) code DYNA3D[6], and coupled with an orthotropic elastic strength model and an equation of state. The full source code for LLNL-DYNA3D is available at Cranfield through a collaboration agreement with LLNL.

4. Coupling of EOS with the proposed stress decompositions

To mathematically describe the propagation of strong shock waves in solids it is necessary to use an EOS in addition to the conservation laws. Basically, an EOS provides a relationship between pressure, density and internal energy. Hence, EOS represents a closure equation, which completes the relationships between the state variables in front of and behind a shockwave. The internal energy is a function of the work done by the stresses. This has as a consequence the coupling of internal energy, pressure, and deviatoric stresses resulting in a nonlinear problem.

In contemporary hydrocodes available EOS's are either of an analytical or a tabulated type. In this paper the Mie-Gruneisen EOS[7,8] implemented in LLNL--DYNA3D was used, this an analytic EOS frequently used when modelling solid materials. It defines the pressure as a function of density ρ and specific internal energy e.

$$P_{EOS} = \frac{\rho_0 c^2 \mu \left[1 + \left(1 - \frac{\Gamma}{2} \right) \mu - \frac{\Gamma}{2} \mu^2 \right]}{\left[1 - (S_1 - 1)\mu - S_2 \frac{\mu^2}{\mu + 1} - S_3 \frac{\mu^3}{(\mu + 1)^2} \right]^2} + (1 + \mu) \cdot \Gamma \cdot e \qquad \text{when } \mu > 0$$

$$P_{EOS} = \rho_0 c^2 \mu + (1 + \mu) \cdot \Gamma \cdot e \qquad \text{when } \mu < 0$$

Where: e is the internal energy per initial unit volume,

$\mu = \frac{\rho}{\rho_0} - 1$ is relative change of volume,

c is the intercept of the U - u_p curve (U - shock velocity vs. u_p particle velocity curve),

S_1, S_2, S_3 are the coefficients of the slope of the U - u_p curve [7,8],

γ_0 is Gruneisen gamma for un-deformed material,

a is the first order volume correction to γ_0,

c, S_1, S_2, S_3, γ_0, a, ρ_0 represent the material properties which must be supplied by the analyst.

The steps taken to couple the EOS with the proposed stress decompositions are described below. The entire stress update algorithm is performed in the local material coordinate system for each element.

4.1 Stress update for the ψ decomposition

Step 1

Calculate material stiffness matrix **C** from material properties read from the input file. Calculate ψ_{ij} using equation (10).

Step 2

Calculate the deviatoric stress increment using the current rate-of-deformation tensor $\dot{\varepsilon}^{n+\frac{1}{2}}$ calculated by DYNA3D and calculate the deviatoric stress at the next time step, $\tilde{s}_{ij}^{n+1}$.

$$\tilde{s}_{ij}^{n} = \sigma_{ij}^{n} + \tilde{P}^{n} \psi_{ij} \tag{26}$$

$$\Delta\sigma_{ij}^{tr\, n+\frac{1}{2}} = C_{ijkl} \dot{\varepsilon}_{kl}^{n+\frac{1}{2}} \Delta t^{n+\frac{1}{2}} \tag{27}$$

$$\Delta\tilde{s}_{ij}^{n+\frac{1}{2}} = \Delta\sigma_{ij}^{tr\, n+\frac{1}{2}} - \frac{\Delta\sigma_{kl}^{tr\, n+\frac{1}{2}} \psi_{kl}}{3} \psi_{ij} \tag{28}$$

$$\tilde{s}_{ij}^{n+1} = \tilde{s}_{ij}^{n} + \Delta\tilde{s}_{ij}^{n+\frac{1}{2}} \tag{29}$$

Step 3

Define a stress σ_{ij}^{n+1} at the next time step, using P_{EOS} as the scalar result from the DYNA3D evaluation of the equation of state, by setting $\tilde{P}$ as in equation (30)

Set $\tilde{P} = P_{EOS}$ (30)

The stress at time step $n+1$ can be updated using equation (31) below

So $\sigma_{ij}^{n+1} = \tilde{s}_{ij}^{n+1} - P_{EOS}^{n+1} \psi_{ij}$ (31)

4.2 Stress update for the ζ decomposition

Step 1

Calculate material compliance matrix **B** from material properties read from the input file. Calculate ζ_{ij} using equation (22).

Step 2

$$\underset{\sim}{s}_{ij}^{n} = \sigma_{ij}^{n} + \underset{\sim}{P}^{n}\zeta_{ij} \tag{32}$$

$$\Delta\sigma_{ij}^{tr\ n+½} = C_{ijkl}\dot{\varepsilon}_{kl}^{n+½}\Delta t^{n+½} \tag{33}$$

$$\Delta\underset{\sim}{s}_{ij}^{n+½} = \Delta\sigma_{ij}^{tr\ n+½} - \frac{\Delta\sigma_{kl}^{tr\ n+½}\zeta_{kl}}{3}\zeta_{ij} \tag{34}$$

$$\underset{\sim}{s}_{ij}^{n+1} = \underset{\sim}{s}_{ij}^{n} + \Delta\underset{\sim}{s}_{ij}^{n+½} \tag{35}$$

Step 3

Define σ_{ij}^{n+1} using P_{EOS} as the scalar result from DYNA3D evaluation of the equation of state. By setting $\underset{\sim}{P}$ as in equation (36)

Set $\underset{\sim}{P} = P_{EOS}$ (36)

The stress at time step $n+1$ can be updated using equation (37) below

So $\sigma_{ij}^{n+1} = \underset{\sim}{s}_{ij}^{n+1} - P_{EOS}^{n+1}\zeta_{ij}$ (37)

The stress decompositions described above were incorporated into DYNA3D[6] and coupled with an orthotropic elastic model and the Mie-Gruneisen EOS.

5. Experimental validation

Two plate impact tests on composite targets[2-4], manufactured from woven carbon fibre-epoxy plies, have been used for model validation. One plate impact test was an impact normal to the fibre direction where shock wave propagated through the thickness of the composite material. The other test was an impact parallel to the one of the fibre directions, where shock waves propagated in the longitudinal direction. In both cases, the carbon fibre composite target plate was modelled as a quasi-orthotropic material. The equivalent material properties of the woven composite plate were determined from the layer macro mechanical properties given in Table 1. for the lay up $[0/90, \pm45]_4$. The longitudinal speed of sound was $C_0 = 3020 ms^{-1}$ for the initial material density $r_0 = 1500 kg/m^3$.

Table 1. Mechanical properties of Carbon Fibre/Epoxy Composite

Density	1500 kg/m^3
Elastic modulus in longitudinal direction E_a	68.457 GPa
Elastic modulus in longitudinal direction E_b	66.527 GPa
Elastic modulus in longitudinal direction E_c	10.0 GPa
Poisson's ratio υ_{ba}	0.0039
Poisson's ratio υ_{ca}	0.0044

Poisson's ratio υ_{cb}	0.0045
Shear modulus G_{ab}	4.57 GPa
Shear modulus G_{bc}	3.57 GPa
Shear modulus G_{ca}	3.57 GPa

A schematic representation of the finite element models of the plate impact tests are shown in Fig. 2 and Fig. 3. It should be noticed that the **a** and **b** directions of the material properties defined in Table 1. correspond to the **x** and **y** coordinate axes for the through thickness impact while in the other case, **a** and **b** correspond to the **z** and **y** coordinate axes respectively.

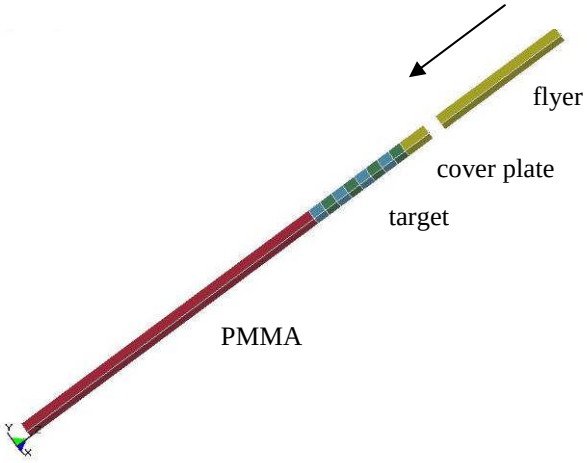

FIGURE 2. The FE Model used to simulate plate impact through thickness of the composite plate

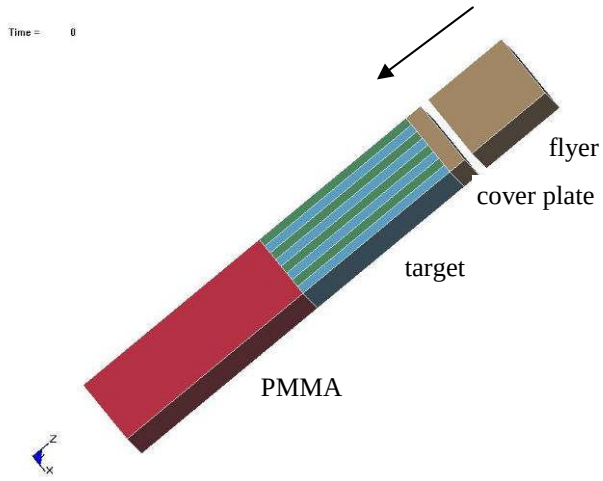

FIGURE 3. The FE Model used to simulate plate impact in the longitudinal direction

The tests involved metal flyer plates impacting a target with a surface metal cover of the same material as the flyer and a rear, thick polymethylmethacrylate (PMMA) backing. The plate impact tests were modelled using a uniaxial strain state under the assumption that the deformation process is adiabatic. Symmetry boundary conditions were applied to all free surfaces parallel to the impact direction and a non-reflective boundary was applied to the back of PMMA-block. The material and velocities of the flyer plate, dimensions of the flyer and target plates as well as the mesh resolution differed between the two

simulations and will be separately defined for each case. A surface to surface contact algorithm was used at the flyer target interface.

5.1 Through Thickness Impact

The aluminium alloy flyer plate was assigned the initial velocity of 504 m/s, as measured in the experiment[2,3]. The flyer plate was 5 mm thick and it was modelled with 30 elements while the test specimen was modelled with 142 elements along the impact axis. This mesh resolution was sufficient to model formation and propagation of the shockwaves. In the experiment the front gauge was covered with a 1 mm aluminium alloy plate while the rear gauge was backed with 12 mm of PMMA. The thickness of the composite plate specimen was 3.8mm.

Aluminium was modelled using an elastic-plastic hydrodynamic model (material 10) with material properties: initial density $r_0 = 2703 kg/m^3$, shear modulus, $G = 27.6 GPa$ and yield strength $Y = 290 MPa$. The parameters for the Mie-Grüneisen EOS had the following values: $c = 5240 \frac{m}{s}$, $S_1 = 1.4$, $S_2 = 0$, $S_3 = 0$, $\gamma_0 = 1.97$, $a = 0.48$. The data for PMMA was taken from the literature[7]. The carbon fibre epoxy target plate was modelled as a quasi-orthotropic material with the properties given in Table 1. The EOS data for the composite material used in the model was: $c = 3230 m/s$, $S_1 = 0.92$, $S_2 = 0$, $S_3 = 0$, $\gamma_0 = 0.84$, $a = 0.50$ (must add an explanation of the source of these figures).

Stress along the axis of impact (the *Z* axis) obtained by decomposition 1 (ψ) and decomposition 2 (ζ) as well as the results obtained using Anderson's model[9] are shown in Fig. 4 and Fig. 5. Stress in the *Z* direction at the front surface of the composite material is compared with the stress history from the front gauge whilst stress in PMMA is compared with the measurements from the rear gauge. The results obtained using decomposition 1 show a good agreement of the stress magnitude and the pulse length with corresponding experimental measurements. Decomposition 2 significantly overestimates the stress in the composite material. Furthermore the simulation based on the decomposition 2 incorrectly predicts separation of the flyer plate from the cover plate, while the decomposition 1 agrees with the experiment, i.e. the flyer plate stays in contact with the cover plate. In Fig. 4 and Fig. 5 it can be clearly seen that Anderson's model overestimates the longitudinal stress level as well as predicting separation of the flyer from the cover plate.

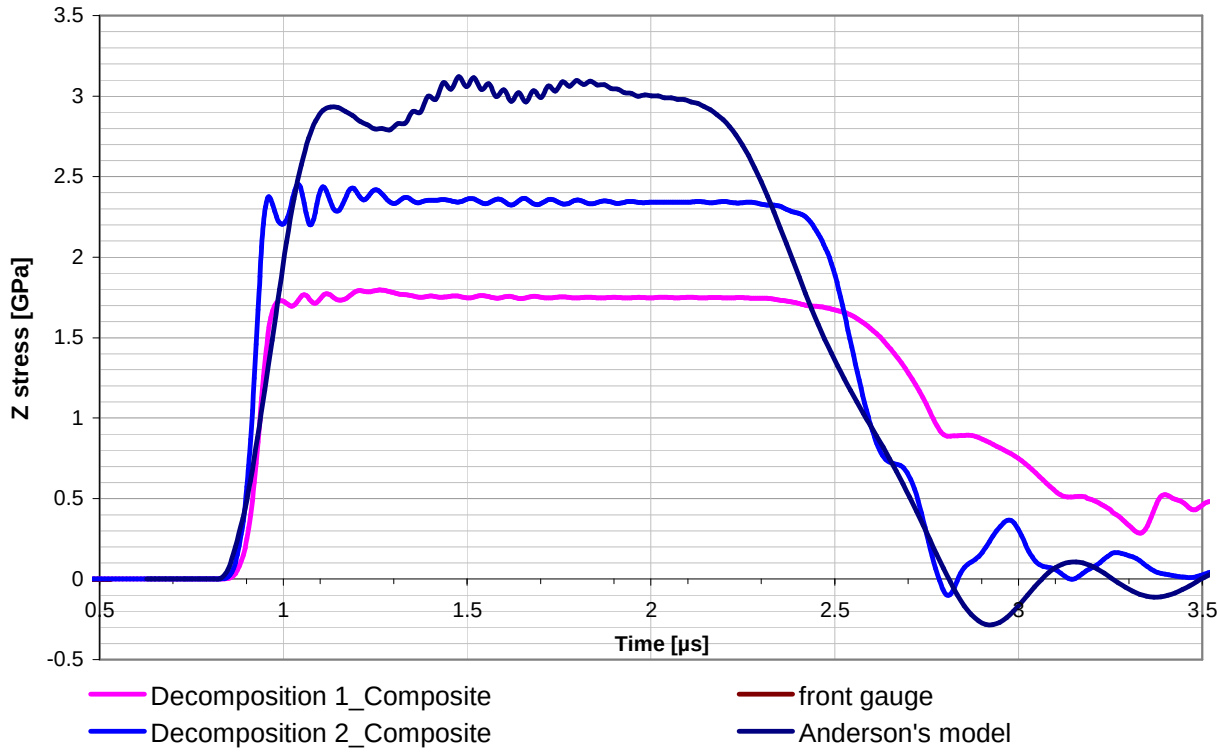

FIGURE 4. Stress traces from the front gauge and results obtained by decomposition 1, decomposition 2 and Anderson's model

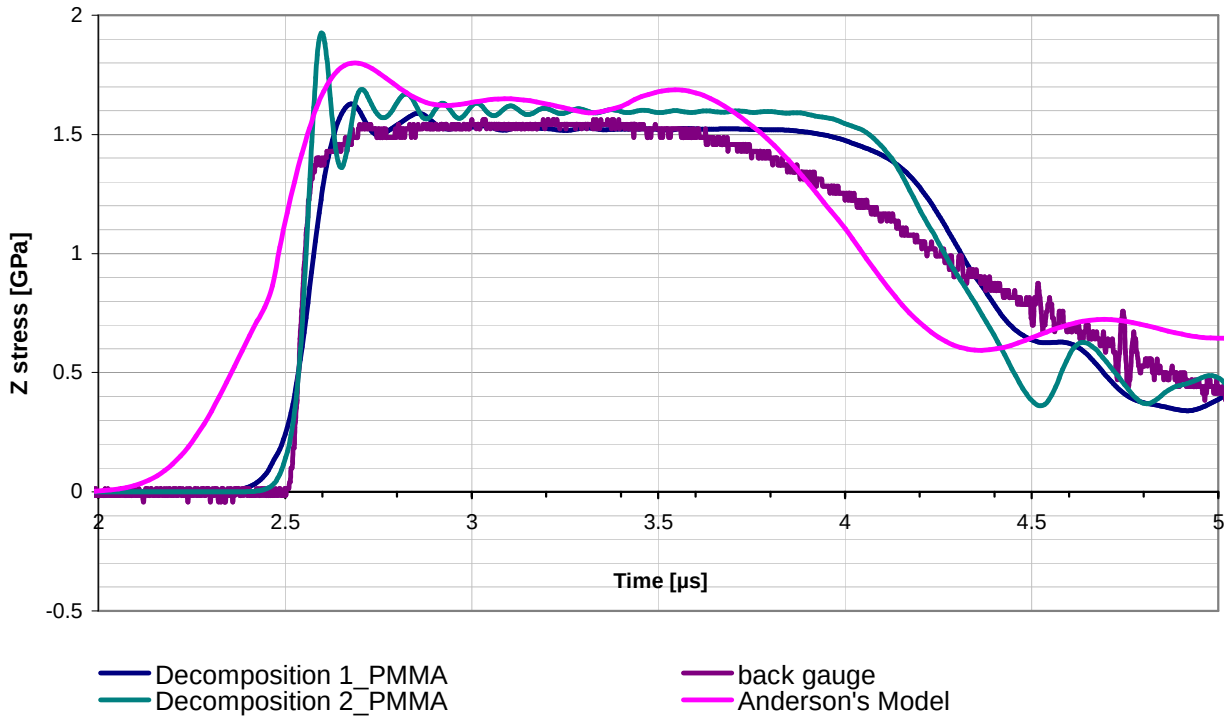

FIGURE 5. Stress traces from the back gauge and results obtained by decomposition 1, decomposition 2 and Anderson's model

5.2. Longitudinal Impact

The FE model used for simulations of the plate impacts in plane of fibre reinforcement is shown

in Fig. 3. This model corresponds to the experimental setup used by Millet[3]. For these simulations only decomposition 1 was used, following the good agreement with the experimental data seen in the through thickness simulations.

Two further tests using different flyer plate materials were performed; one with a copper flyer plate and the other with a tungsten flyer plate. Furthermore, two different composite specimen thicknesses, 6 mm and 10 mm, were tested with the copper flyer plate. In all these experiments, 12 mm thick PMMA backing plates and 1 mm thick cover plates on the specimen were used.

The initial velocity of the copper flyer plate was 940 m/s, for both specimen thicknesses, as reported for the experiments[3]. The flyer plate was 5mm thick and modelled with 10 elements along the impact axes. The 10 mm composite was modelled with 48 elements while the 6mm specimen was modelled with 40 elements along the impact axis. The tungsten flyer plate had an initial velocity of 927 m/s as reported for the experiments[3]. The flyer plate was 5mm thick and it was modelled with 10 elements while the test specimen was modelled with 48 elements along the impact axis. Material properties and parameters for the Mie-Grüneisen EOS of the OHFC copper and tungsten were taken from[7] and are given in Table 2. The flyer plate was modelled with Johnson Cook material model.

Table 2. Mechanical properties of OFHC copper and tungsten used in simulations

Material	**OFHC copper**	**Tungsten (WHA)**
Density	8930 kg/m^3	18200 kg/m^3
Shear modulus, G	47.7 GPa	160 GPa
Yield stress constant, A	120 MPa	2.2 GPa
Strain hardening coefficient, B	292 MPa	2.92 GPa
Strain hardening exponent, n	0.31	0.19
Strain rate dependent coefficient, C	0.025	0.025
Temperature dependence exponent, m	1.09	1.09
Melt temperature, T_m	1790	4520 K
Room temperature, T_r	293	293 K
Reference strain rate,	1.00	1.00
Specific heat, c_v	383 J/kgK	129 J/kgK
Failure stress	1.20 GPa	1.20 GPa
EQUATION OF STATE Mie Gruneisen		
C_O	3940 m/s	4030 m/s
S_1	1.489	1.237
S_2	0	0

S_3	0	0
γ_0	2.02	1.67
a	0.47	0.38

The carbon fibre composite target plate was modelled as a quasi-orthotropic material with the properties given in Table 1. The EOS data for the composite material used in the model was: $c = 3230 m/s$, $S_1 = 0.92$, $S_2 = 0$, $S_3 = 0$, $\gamma_0 = 0.84$, $a = 0.50$.

In the case of the through thickness test and simulation, the shock front is planar and parallel to the composite plies. Consequently the stress measured by the gauge and the stress in the corresponding finite elements is directly comparable. In the case of longitudinal impact the shock front is not planar due to the different ply orientations. Consequently the gauge measures averaged stresses over a number of plies. Each composite ply was 0.475mm thick, while the gauges were 5mm long and at 45º relative to the plies. Therefore it was necessary to average the stress at the gauge locations in the simulations to allow for comparison with the experimental data. Here only the results from the back of the specimens are shown because of uncertainty in the experimental results from the front gauge.

The stress along the axis of impact (Z axes) at the back of the specimen was obtained for the impact of a copper flyer plate on 6 mm and 10 mm specimens, shown in Fig. 6. These results are compared to the experimental rear surface gauge histories[3]. The results show good agreement in the stress magnitude and the pulse length with the corresponding experimental measurements. There are clear differences in the rising part of the curves, especially for the 10 mm specimen, which are not fully understood. They could be due to the measurement technique used in the experiments and some physical processes occurring in the composite that are not captured by the model. The end of the numerically obtained pulse differs from the experiment, likely due to the fact that material damage, observed in the experiments is not considered in the simulations. An additional source of the discrepancy could be the difference in averaging of the stress in the gauges and in the numerical simulations along with loss of uniaxial strain at late times.

Numerical results and a rear surface gauge history for the impact of the tungsten alloy flyer plate are shown in Fig. 7. This result shows better agreement in the stress magnitude and in the pulse length with the experimental curves compared to the results for the copper plate impact. There is still difference in the rising part of the slopes, but the magnitude of the pulse seems the same.

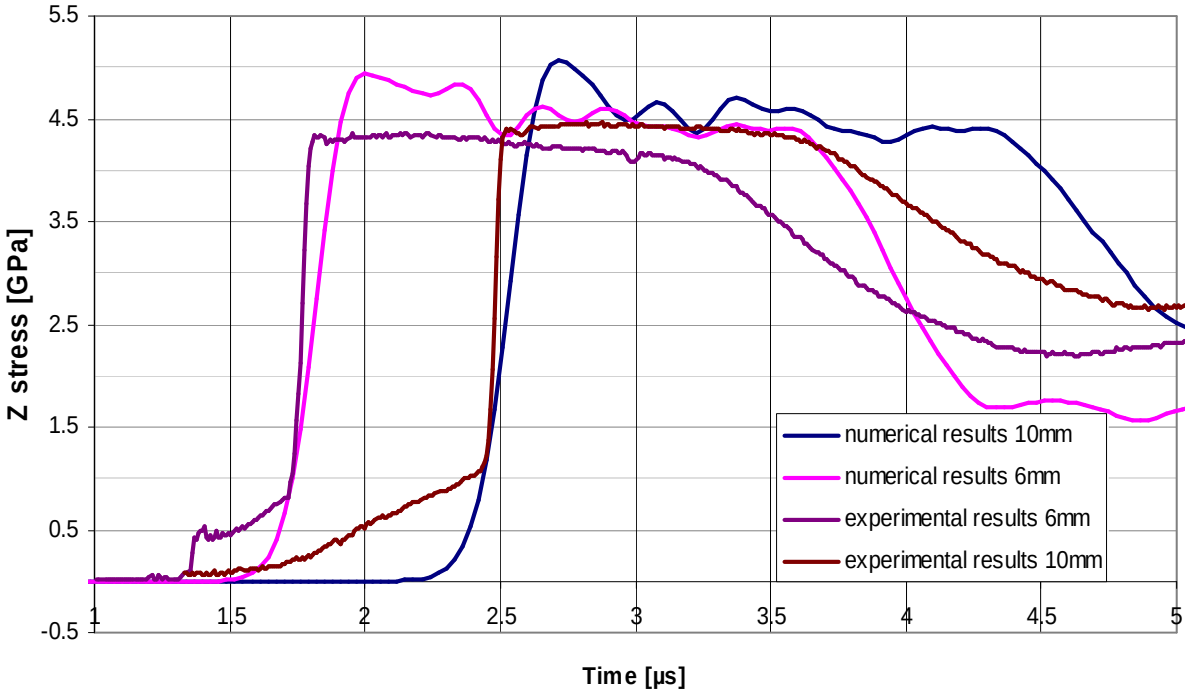

FIGURE 6. Stress traces from the rear surface gauge and obtained results for the copper impact plate; 6mm and 10mm specimens

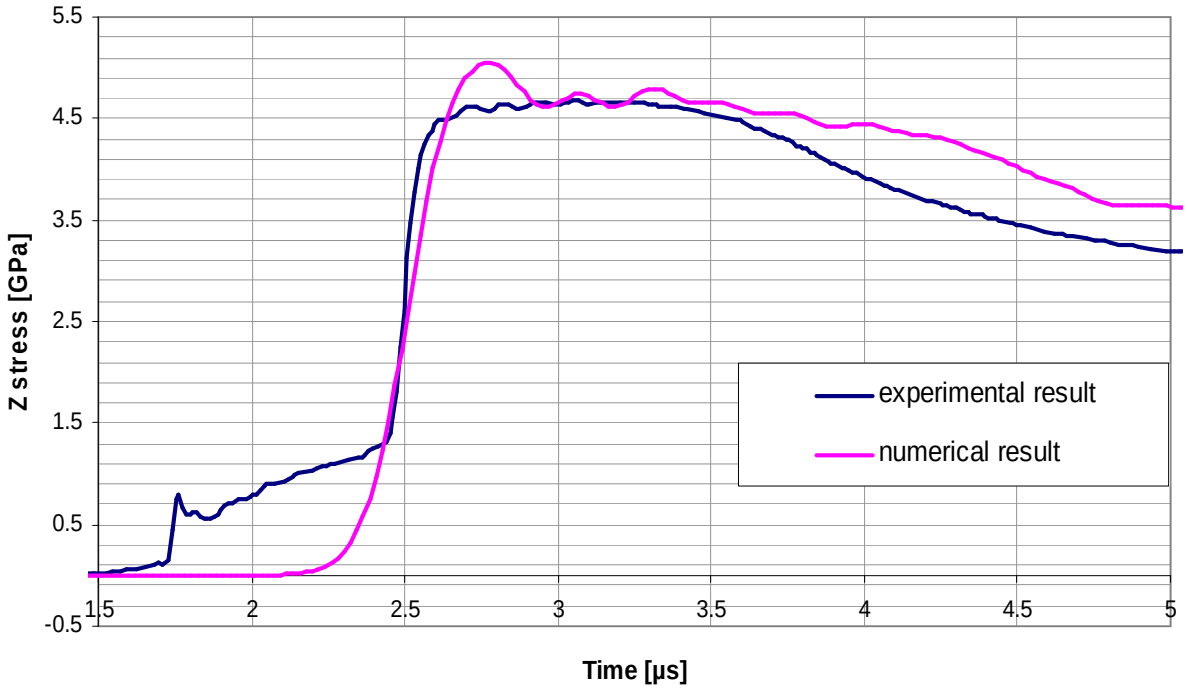

FIGURE 7. Stress traces from the rear gauge and obtained results for the tungsten impact plate; 10mm specimen

6. Summary

As observed by Anderson[1] the shock response of an orthotropic material can not be accurately predicted using the conventional decomposition of the stress tensor into isotropic and deviatoric parts. This paper presents two different stress decompositions based on the assumption that the stress tensor is

split into two components; one component due to volumetric strain and the other due to deviatoric strain, instead of volumetric stress and deviatoric stress. Both decompositions are rigorously derived. In order to test their ability to describe shock propagation in orthotropic materials, both algorithms were implemented in a hydrocode and their predictions compared with experimental plate impact data. The material considered was a carbon fibre reinforced epoxy material which was tested in both the through-thickness and longitudinal directions.

The two decompositions were validated against the through thickness experimental data. The ψ decomposition showed good agreement with the physical behaviour of the considered material while the ζ decomposition significantly overestimated the longitudinal stresses. The experimental curves were also compared with predictions made using the decomposition proposed by Anderson, which significantly overestimated the longitudinal stress.

The ψ decomposition was then used to simulate three plate impact tests in the longitudinal direction. The simulation results showed good agreement with the experimental data. Differences between the experimental traces and numerical results in these test cases could be a consequence of the orientation and position of the gauges related to the lay up of the composite material as well as the gauge averaging the recorded stress across its area. Thus an important feature of further validation would be to such simulations should be to improve the understanding of the experimental averaging occurring in the gauge so that it can be replicated in the simulation.

Acknowledgment
The authors would like to acknowledge that this work was part-funded by the UK Engineering and Physical Sciences Research Council (EPSRC) Grant Reference: GR/S33956/01
The authors would like to thank Professor Stephan Hiermaier, Ernst Mach Institute, Freiburg, for his constructive comments and suggestions during this work.

7. References

[1] Anderson, C. E., Cox, P. A., Johnson, G.R., Maudlin, P. J., A Constitutive Formulation for Anisotropic Materials Suitable for Wave Propagation Computer program-II, Comp. Mech., 1994, vol. 15, p. 201-223.

[2] Vignjevic, R., Millett, J.C.F., Bourne, N.K., Meziere, Y., and Lukyanov, A., *The Behaviour of a Carbon-Fibre Epoxy Composite under Shock Loading*, in Shock Compression of Condensed Matter 2005, Furnish, M.D., Elert, M.L., Russell, T.P., and White, C.T., Editors. 2006, American Institute of Physics: Melville, New York. p. 825-828.

[3] J.C.F. Millett, N.K. Bourne, R. Vignjevic, Y.J.E. Meziere, A. Lukyanov; *The effect of orientation on the shock response of a carbon fibre - epoxy composite*, Composite Science and Technology (2007) In press

[4] Millett J. C. F. and N. K. Bourne, The behavior of an epoxy resin under one-dimensional shock loading. Journal of Applied Physics 92 (11), 2002, 6590-6594.

[5] Bourne, N.K., Stevens, G.S., A gas gun for plane and shear loading of inert and explosive targets. Rev. Sci. Instrum. 72(4), 2001., 2214-2218.

[6] Hallquist J. O., Whirley R. G., DYNA3D User manual, Nonlinear dynamic analysis in three dimensions. University of California, Lawrence Livermore National Laboratory, Report UCID-19592, 1989. Rev. 5.

[7] Steinberg D. J., 1991. Equation of State and Strength Properties of Selected Materials, Report No. UCRL-MA-106439, Lawrence Livermore National Laboratory, Livermore, CA

[8] Gruneisen E, The State of Solid Body, NASA R19542, 1959

[9] Hiermaier S, Structures Under Crash and Impact, Springer Science, 2008

Modeling shock waves in orthotropic elastic materials

Vignjevic, Rade

2008-08-01

Vignjevic, R., Campbell, J.C., Bourne, N.K. and Djordjevic, N. 2008. Modeling shock waves in orthotropic elastic materials. Journal of applied physics, 104(4), article 044904.
http://dx.doi.org/10.1063/1.2970160